Rapid Binding of T7 RNA Polymerase Is Followed by Simultaneous Bending and Opening of the Promoter DNA†

Guo-Qing Tang and Smita S. Patel*

Department of Biochemistry, University of Medicine and Dentistry of New Jersey-Robert Wood Johnson Medical School, 675 Hoes Lane, Piscataway, New Jersey 08854

Received November 8, 2005; Revised Manuscript Received January 31, 2006

ABSTRACT: To form a functional open complex, bacteriophage T7 RNA polymerase (RNAP) binds to its promoter DNA and induces DNA bending and opening. The objective of this study was to elucidate the temporal coupling in DNA binding, bending, and opening processes that occur during initiation. For this purpose, we conducted a combined measurement of stopped-flow fluorescence anisotropy, fluorescence resonance energy transfer (FRET), and 2-aminopurine fluorescence. Stopped-flow anisotropy measurements provided direct evidence of an intermediate resulting from rapid binding of the promoter to T7 RNA polymerase. Stopped-flow FRET measurements showed that promoter bending occurred at a rate constant that was slower than the initial DNA binding rate constant, indicating that the initial complex was not significantly bent. Similarly, stopped-flow 2-aminopurine fluorescence changes showed that promoter opening occurred at a rate constant that was slower than the initial DNA binding rate constant, indicating that the initial complex was not significantly melted. The indistinguishable observed rate constants of FRET and 2-aminopurine fluorescence changes indicate that DNA bending and opening processes are temporally coupled and these DNA conformational changes take place after the DNA binding step. The results in this paper are consistent with the mechanism in which the initial binding of T7 RNAP to the promoter results in a closed complex, which is then converted into an open complex in which the promoter is both sharply bent and melted.

Bacteriophage T7 RNA polymerase (RNAP)[1] is a single-subunit enzyme that is capable of catalyzing all the fundamental steps of transcription without requiring any accessory proteins (*1*, *2*). Although the T7 RNAP structure is more closely related to the Pol I family of DNA polymerases rather than to the multisubunit bacterial or eukaryotic RNA polymerases, the fundamental mechanism of RNA-dependent transcription is conserved in both single- and multiple-subunit RNAPs (*3*−*9*). After T7 RNAP recognizes and binds to a specific sequence of DNA, a series of conformational changes occur in both the promoter DNA and RNAP that result in sequence specific RNA synthesis. In the initial process of promoter DNA binding, a key step is the melting of the DNA duplex around the initiation site to create a single-stranded DNA for template-directed RNA synthesis. DNA in the open complex is not only melted from −4 to +2/+3 (*10*) but also bent around the transcription start site (*11*, *48*).

The mechanism by which RNAPs melt a specific region of the promoter DNA is not well understood, mainly because the initial steps of promoter recognition and DNA binding are poorly characterized. Minimally, these steps should include the formation of a closed complex and intermediates that initiate promoter melting. Previously, we have used 2-aminopurine (2-AP)-modified fluorescent DNA to monitor the real-time kinetics of open complex formation under pseudo-first-order conditions (*12*−*14*). On the basis of these kinetic and thermodynamic studies as well as global fitting of the kinetic data, we proposed a minimal two-step mechanism in which open complex formation occurs via a kinetic intermediate that we termed the closed complex intermediate (*13*). This model extended an initial mechanism that proposed rapid promoter opening is simultaneous with promoter binding (*12*, *15*). Additional studies indicated that the closed and open complexes of the duplex promoter are in equilibrium, with the closed complex being favored until initiating nucleotides are added, which stabilizes the ternary open complex (*16*).

Using steady-state and time-resolved FRET methods, we have determined that the overall bending angle of the promoter DNA in the static open complex is ∼80° (*48*). Equilibrium FRET studies indicated that the initial closed complex is not bent to a significant extent. The following questions arise: whether DNA bending is simultaneous with DNA binding and whether an intermediate in which the DNA is bent but not melted exists. Although there is no direct evidence, it is generally thought that promoter DNA bending induced upon RNAP binding occurs prior to promoter DNA melting (*17*−*20*). In many proteins such as the minor groove intercalating TATA-binding protein (TBP) (*21*, *22*), the

† This project is funded by NIH Grant GM51966 to S.S.P.

* To whom correspondence should be addressed. E-mail: patelss@umdnj.edu. Telephone: (732) 235-3372. Fax: (732) 235-4783.

[1] Abbreviations: 2-AP, 2-aminopurine; A488, succinimidyl ester of 5(6)-Alexa Fluor 488 carboxylic acid; A546, succinimidyl ester of 5(6)-Alexa Fluor 546 carboxylic acid; FRET, fluorescence resonance energy transfer; NT, nontemplate strand; RNAP, RNA-dependent polymerase; pds, partially double-stranded DNA; T, template strand; TAMRA, tetramethylrhodamine.

10.1021/bi052292s CCC: $33.50
Published on Web 03/22/2006

chromosomal high-mobility group proteins (HMG) (*23*), and the integration host factor (IHF) (*24*), DNA binding and bending are synchronous events. For DNA-modifying enzymes such as methyltransferases and DNA repair endonucleases (*25*−*28*) that recognize and act at specific sites on the DNA, it was observed that DNA binding, bending, and/or base flipping occurred as a concerted event. Recently, Stivers and colleagues argued that DNA bending might take place earlier and facilitate base flipping in the DNA bound to uracil DNA glycosylase (*29*).

In this paper, we have used stopped-flow fluorescence anisotropy to directly assess the initial step of T7 RNAP−promoter DNA association. A "three-color" DNA substrate was synthesized with donor and acceptor dyes at the DNA ends, and a fluorescent base 2-AP at the −4 position in the template strand. The three-color promoter was used to compare directly the rate constants of DNA bending and opening and that of DNA binding to investigate the multistep mechanism of promoter melting during transcription initiation. Stopped-flow FRET and 2-AP fluorescence changes indicated that promoter bending and DNA opening are temporally coupled during initiation by T7 RNAP. The intrinsic rate constants of steps were determined from the kinetics of binding, bending, and opening with a duplex and a premelted promoter, both in the absence and in the presence of the initiating nucleotides. The development of these methods and the successful application to T7 RNAP provide ways to study the early events of transcription initiation in other polymerases. This approach will be particularly useful for RNAPs in which 2-AP substitution may have a deleterious effect on transcription of certain promoters (*30*).

MATERIALS AND METHODS

Protein and DNA. T7 RNAP was purified as described previously (*12*, *31*), and the protein concentration was determined by measuring the absorbance at 280 nm in 8 M urea using a molar extinction coefficient of 1.4×10^5 M^{-1} cm^{-1} (*32*). Oligodeoxynucleotides were purchased from Integrated DNA Technologies, Inc. (Coralville, IA). The sequence of NT was 5′-TAA ATT AAT ACG ACT CAC TAT AGG GAG ACT A, that of T 3′-ATT TAA TTA TGC TGA GTG ATA TCC CTC TGA T, and that of mutNT 5′-TAA ATT AAT ACG ACT CAC CCG CAT GAG ACT A. DNA purification, dye labeling [Alexa 488 (A488) and Alexa 546 (A546)], and labeling analysis were as described in ref *48*. Fluorescent base analogue 2-aminopurine (2-AP) was incorporated at position −4 on the template strand during oligodeoxynucleotide synthesis. Duplex DNA was prepared by annealing two fluorescent strands in an equimolar ratio to make a doubly labeled promoter DNA or by adding a 5% excess of the nonfluorescent strand to make a singly dye-labeled DNA.

Stopped-Flow Fluorescence Anisotropy Experiments. Time-dependent measurement of fluorescence anisotropy changes in the Alexa 546-modified promoter upon binding to T7 RNAP was performed in a T-format setup on a KinTek SF-2003 instrument (KinTek Corp., Austin, TX) equipped with computer-controlled motor-driven syringes. The fluorescence signals were collected in 1000 channels with a dead time of 1−2 ms. Excitation light at 550 nm was transmitted via a fiber-optic output into an optical sample cell. The emission signal was passed through 570 nm long-pass filters and measured simultaneously in parallel and perpendicular orientation relative to the polarized excitation. All the measurements were carried out in a buffer containing 50 mM Tris-acetate, 50 mM Na-acetate, 10 mM Mg-$(acetate)_2$, and 1 mM dithiothreitol (pH 7.5). Duplex promoter labeled with A546 (final concentration of 40 nM) was mixed with T7 RNAP (from 50 to 800 nM, final concentration). The polarized emission signal from 10−15 shots was averaged to improve the signal-to-noise ratio. Differences in the sensitivity between the two photomultipliers were adjusted to calculate the anisotropy of DNA-labeled A546. The observed anisotropy was calculated using eq 1:

$$r_{obs} = \frac{I_{||}/I_{\perp} - 1}{I_{||}/I_{\perp} + 2} \quad (1)$$

At any given time during the DNA binding event, the observed fluorescence anisotropy, r_{obs}, of DNA-labeled A546 is the sum of free and RNAP-bound DNA:

$$r_{obs} = r_b f_b + r_f f_f \quad (2)$$

where f_f and f_b are fractions of unbound and bound DNA, respectively, relative to total fluorescent DNA ($f_f + f_b = 1$) and r_f and r_b are their respective anisotropy values. The general equation used to fit the time-dependent anisotropy changes is shown in eq 3

$$r_{obs} = r_b + \frac{r_f - r_b}{1 - \alpha + \alpha e^{kt}} \quad (3)$$

where α ($=I_{bound}/I_{free}$) is a correction factor in case the fluorescence intensity (I) changes upon complex formation and k is the observed rate constant. Binding to T7 RNAP did not cause any significant changes in the total fluorescence intensity of A546 attached to the promoter DNA. Therefore, $\alpha = 1$ and eq 3 is simplified to $r_{obs} = \Delta r e^{-kt} + \text{constant}$. The observed rate constant (k) was plotted against T7 RNAP concentration, and the dependency was fit to eq 4 to obtain the on-rate constant (k_{on})

$$k_{obs} = k_{on}[E]_t + k_{off} \quad (4)$$

Stopped-Flow FRET Experiments. Rapid assays of T7 RNAP-induced FRET changes upon DNA binding were conducted on the same KinTek SF2003 setup. Doubly dye-labeled promoter (final concentration of 20−40 nM) was rapidly mixed with T7 RNAP (from 100 to 800 nM, final concentration), and fluorescence intensities of both donor and acceptor dyes were measured simultaneously in a T-format setup. A 520 nm band-pass filter was used to measure the emission fluorescence intensity of A488 within the 515−525 nm window that excludes emission light from A546. Similarly, a 570 nm long-pass filter was used to collect A546 emission. Fluorescence measurements from 10−15 experiments were averaged to optimize the signal-to-noise ratio. The observed rate constants were obtained by simultaneously fitting the time traces from donor and acceptor fluorescence changes using Sigmaplot (Jandel Scientific Software, San Rafael, CA). Generally, a single-exponential equation (eq 5) provided a satisfactory fit to the data as justified by visible inspection and by the random distribution

of residuals.

$$F = F_0 + \Delta F \exp(-kt) \quad (5)$$

where F is the observed fluorescence intensity, F_0 is the background fluorescence, and ΔF is the fluorescence change during the binding process. The observed rate constant (k) was plotted against T7 RNAP concentration, and the resulting dependency was fit to either a linear equation (eq 4, for the bubble promoter) or a hyperbolic equation (eq 6, for the duplex promoter).

$$k_{obs} = k_{off} + \frac{k_{max}[E]_t}{[E]_t + K_{1/2}} \quad (6)$$

where k_{max} is the maximum rate constant for the unimolecular rearrangement (bending or opening) of promoter DNA as detected by FRET efficiency or 2-AP fluorescence signal, $K_{1/2}$ is a nominal measure of the binding affinity whose meaning is not straightforward, and k_{off} is the rate constant of the reverse reaction.

Stopped-Flow 2-AP Fluorescence Experiments. To compare directly the kinetics of T7 RNAP-induced DNA opening and bending, a three-color DNA promoter was prepared by attaching the A488−A546 dye pair to the DNA ends and labeling the template strand with 2-AP internally at position −4. To minimize interference from A488 and A546 fluorescence, a 400 nm band-pass filter was used to collect 2-AP fluorescence within the 365−435 nm range. Transmittance measurements using the 400 nm band-pass filter indicated a complete blockage of >480 nm light. Experimental conditions and data analyses were the same as those described above for the stopped-flow FRET experiments.

RESULTS AND DISCUSSION

Real-Time Analysis of Promoter Association by Stopped-Flow Fluorescence Anisotropy. A 31 bp DNA with the T7 Φ10 promoter sequence from position −22 to +9 was labeled with A546 at the 5′-end of the template DNA. Fluorescence anisotropy changes under equilibrium conditions were measured by titrating the dye-labeled duplex promoter with an increasing T7 RNAP concentration. The anisotropy of the dye attached to the duplex promoter increased from ∼0.16 in the absence of T7 RNAP to ∼0.20 in the fully bound state (Figure 1). The binding data were fit to obtain the T7 RNAP−duplex promoter K_d of 5.2 nM, which is consistent with the previously measured value for a consensus T7 promoter with an upstream end at residue −22 (*33*, *34*). Fluorescence anisotropy changes were then measured in a stopped-flow instrument to obtain the kinetics of DNA binding. The A546-labeled duplex promoter was rapidly mixed with an excess of T7 RNAP in a stopped-flow instrument, and the time-dependent increase in fluorescence anisotropy was recorded. Real-time measurements of fluorescence changes of A546 in both parallel ($I_{||}$) and perpendicular ($I_\perp$) directions relative to the vertically polarized excitation were taken using a T-format scheme. The A546-labeled duplex promoter was excited at 550 nm, and the emission intensity at >570 nm was collected using 570 nm cutoff filters. The sensitivity of each of the two photon multiplier tubes (PMT) in response to instrument setting parameters such as excitation and emission wavelengths, excitation slits, and PMT voltages was evaluated and taken into consideration to adjust the ratio of $I_{||}$ and $I_\perp$.

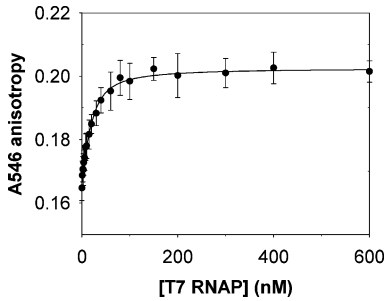

FIGURE 1: Fluorescence anisotropy changes accompanying the binding of A546-labeled duplex promoter under equilibrium conditions. The duplex promoter labeled with A546 (40 nM) was titrated with increasing T7 RNAP concentrations at 20 °C, and fluorescence anisotropy was measured. The dye was excited at 550 nm, and perpendicular and parallel intensities at 585 nm were monitored in a T scheme. Error bars represent deviations in 10 consecutive fluorescence measurements at each protein concentration.

Figure 2A shows a typical fluorescence anisotropy time course when 40 nM A546-labeled duplex promoter was rapidly mixed with 200 nM T7 RNAP (both final concentrations). The final trace is an average of 8−12 experiments and follows a single-exponential equation (eq 3) with a first-order rate constant of 43 s^{-1}. To determine whether the A546 anisotropy signal change is a direct measure of the association of T7 RNAP and promoter DNA, the stopped-flow kinetics were measured under pseudo-first-order conditions at final T7 RNAP concentrations from 80 to 800 nM and a constant dye-labeled promoter concentration of 40 nM. The observed rate constant of anisotropy changes increased linearly with an increase in T7 RNAP concentration (Figure 2B), and the bimolecular promoter association rate constant, k_{on}, was determined from the slope to be 188 ± 5 μM^{-1} s^{-1}. This fast on-rate constant indicates diffusion-limited rapid association of T7 RNAP with the consensus promoter fragment. This directly measured on-rate constant of the T7 RNAP−duplex promoter complex is consistent with the previously estimated value from global fitting of the kinetics of 2-AP fluorescence changes (*13*, *14*, *16*). The off-rate constant of the T7 RNAP−duplex promoter complex can be obtained from the *y*-intercept of the observed rate constant (k_{obs}) versus T7 RNAP concentration linear dependency ($k_{obs} = k_{on}$[T7 RNAP] + k_{off}). However, because the starting concentrations of T7 RNAP were far from zero, the off-rate constant could not be determined accurately by this method. The off-rate constant was determined directly from displacement experiments shown below. From the K_d of 5 nM for this promoter DNA sequence and the simplified relationship $K_d = k_{off}/k_{on}$, the off-rate constant is estimated to be ∼1 s^{-1}.

The stopped-flow fluorescence anisotropy experiments (Figure 2C,D) were also conducted with a premelted promoter (bubble promoter) that contained six contiguous mismatches in the nontemplate strand from position −4 to +2. Binding of the A546-labeled bubble promoter to T7 RNAP resulted in an increase in dye anisotropy. The observed exponential rate constant of binding increased linearly with an increase in T7 RNAP concentration (Figure 2D) and provided an on-rate constant of 299 ± 20 μM^{-1} s^{-1}. This association on-rate constant of the bubble promoter is only slightly higher than the on-rate constant of the duplex

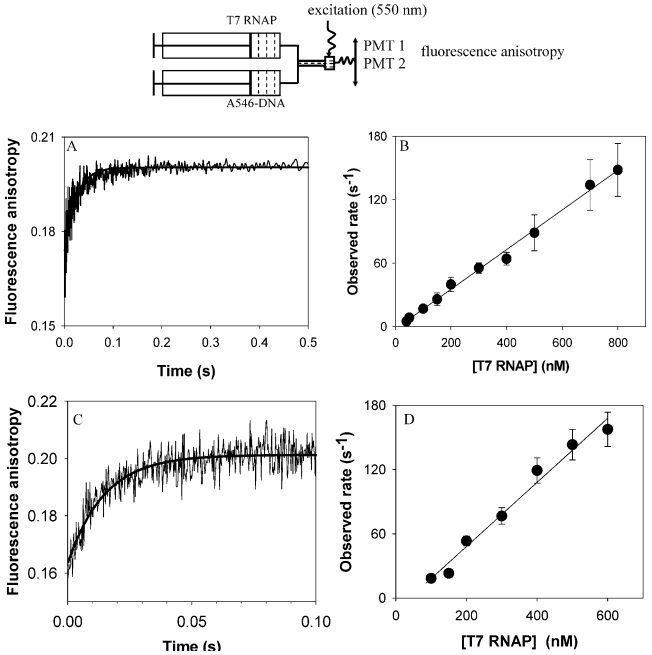

FIGURE 2: Stopped-flow kinetics of duplex and bubble promoter binding measured by fluorescence anisotropy. (A) A546-labeled duplex promoter (NT/Alexa 564-T) at 40 nM (final) was rapidly mixed with 200 nM T7 RNAP (final concentration) at 25 °C in a stopped-flow instrument. The resulting time course of fluorescence anisotropy change that fits to a single-exponential function with a k_{obs} of 43.2 ± 1.5 s^{-1} (smooth curve) is shown. (B) The observed rate constant of anisotropy change is plotted as a function of increasing T7 RNAP concentrations that provided a k_{on} of 188 ± 5 μM^{-1} s^{-1}. (C) A546-labeled bubble DNA (mutNT/T-A546) at 40 nM (final concentration) was rapidly mixed with 200 nM T7 RNAP (final concentration) at 25 °C in a stopped-flow instrument, and the resulting kinetics of fluorescence anisotropy changes are shown. Ten traces were averaged (rugged curve) and fit to a single-exponential function to obtain an observed rate constant (k_{obs}) of 68 ± 13 s^{-1} (smooth curve). (D) Observed rate constants of bubble DNA binding are plotted vs T7 RNAP concentration, and the slope provided a k_{on} of 299 ± 20 μM^{-1} s^{-1}. All anisotropy measurements were made with vertically polarized excitation at 550 nm and by collection of parallel and perpendicular emission at wavelengths longer than 570 nm (using dual 570 nm long-pass filters). The dashed lines in the schematic (here and in the following figures) represent the liquid solution, and the curves represent excitation or emission lights transmitted through fibers.

promoter (~1.5 times). On the other hand, the affinity of the bubble promoter for T7 RNAP is nearly 3 orders of magnitude stronger than that of the duplex promoter (*35*), suggesting that the tight binding of the bubble promoter is due to the greatly reduced off-rate constant (shown below) of the RNAP−promoter complex (*35*).

Real-Time Analysis of DNA Bending and Opening by Stopped-Flow FRET and 2-AP Fluorescence. To dissect the pathway of DNA binding, bending, and base pair opening, a three-color DNA promoter was made with A488 and A546 dyes attached to the opposite ends of the DNA and 2-AP substituted at position −4 in the template (Figure 3). Unstacking of the 2-AP base at the −4 position on the template strand occurs upon promoter DNA melting, and the accompanying fluorescence increase has been exploited to characterize the thermodynamics and kinetics of open complex formation (*12*, *15*, *35*, *36*). By following the real-time fluorescence changes of the 2-AP base, one can assess the formation of the RNAP−promoter open complex (*13*). Similarly, real-time bending of the promoter DNA can be

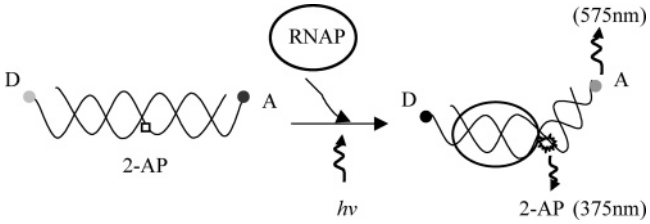

FIGURE 3: DNA bending and opening kinetics measured using a three-color promoter. The DNA promoter was labeled with donor and acceptor dyes at the DNA ends and with 2-AP at position −4 in the template strand. The three-color DNA substrate was used to measure the kinetics of bending and opening as shown in the diagram. The incorporated 2-AP is shown as a white box in the free DNA (less fluorescent) and as an explosion in the complex (highly fluorescent). The upstream and downstream labeled donor (D) and acceptor (A) are colored gray and black in the free DNA and black and gray in the T7 RNAP complex, respectively, corresponding to the FRET enhancement. Fluorescence excitation was set at 315 nm, and changes in the 2-AP fluorescence at wavelengths of >365 nm were measured using a 400 ± 35 nm band-pass filter. With the same DNA, the excitation was moved to 490 nm and simultaneous changes in donor and acceptor fluorescence emission were made in two channels using a 570 ± 5 nm long-pass filter (acceptor side) and a 520 ± 5 nm band-pass filter (donor side), respectively.

measured by monitoring the time-dependent donor and acceptor fluorescence changes that accompany binding of the promoter to T7 RNAP. Thus, the three-color DNA provides a direct and error-minimized comparison of the rates of T7 RNAP-induced DNA bending and opening by the stopped-flow method.

FRET and 2-AP signals were measured with the three-color DNA in a single sample. The 2-AP signal was measured after excitation at 315 nm, and the FRET signal was measured after excitation at 490 nm. A band-pass filter centered at 400 nm with a broad width of 70 nm was used to collect the 2-AP signal, while preventing A488 and A546 fluorescence interference in the long-wavelength region. The changes in donor and acceptor emission were simultaneously monitored with a T-format detection system. A 520 nm band-pass filter was used to measure the emission fluorescence intensity of A488 within the 515−525 nm window that excludes emission light from A546. Similarly, a 570 nm long-pass filter was used to collect A546 emission. Although the binding kinetics by anisotropy can be measured using the same three-color DNA by selectively exciting the acceptor only, the requirement of reassembling several key parts of the stopped-flow setup makes this difficult. However, we confirmed that the three-color and the singly dye-labeled DNA substrates provided similar DNA binding rate constants (data not shown).

Figure 4 shows typical fluorescence changes observed after the mixing of 100 nM T7 RNAP (final concentration) with 40 nM three-color duplex promoter. The time-dependent increase in 2-AP fluorescence is mainly due to base unstacking that accompanies duplex DNA opening, and the kinetics fit to a single-exponential rate constant of 12 s^{-1}. The time-dependent decrease in donor fluorescence and the accompanying increase in acceptor fluorescence measure the kinetics of DNA bending upon T7 RNAP binding. The donor and acceptor signals were fit simultaneously to a single-exponential rate constant of 12 s^{-1}. Thus, the 2-AP fluorescence and the FRET changes occur with similar kinetics. The stopped-flow 2-AP fluorescence and FRET kinetics were

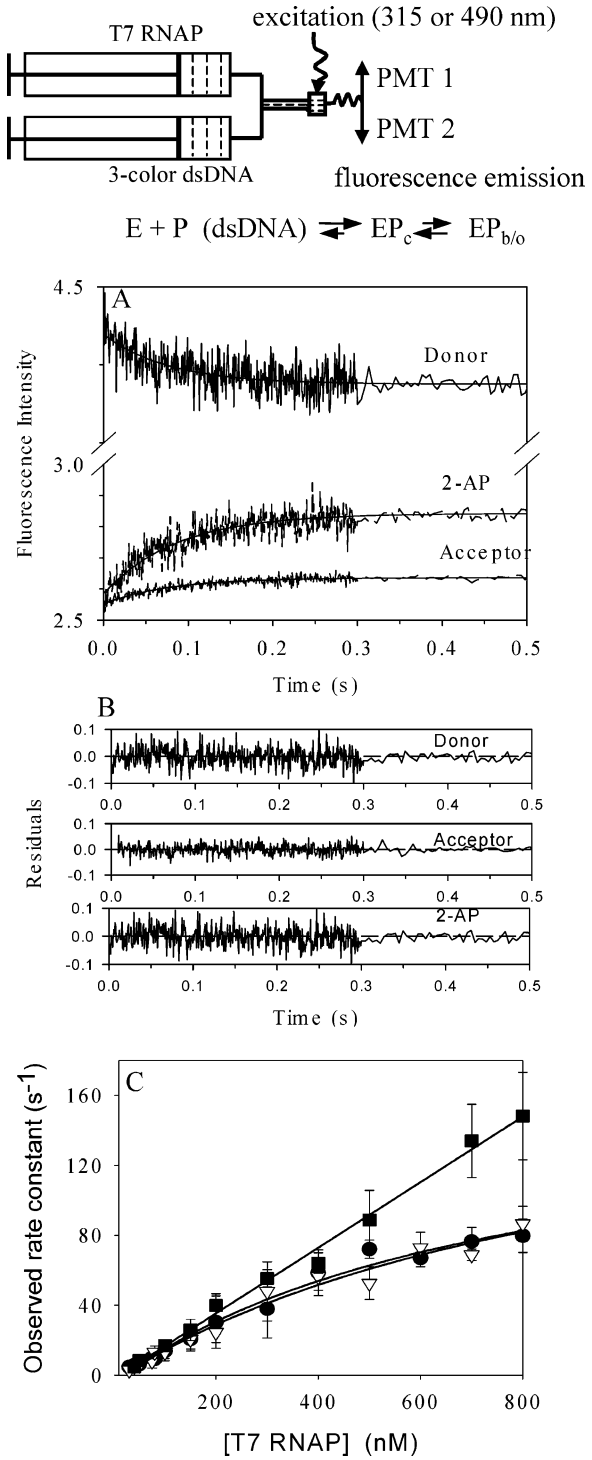

FIGURE 4: Stopped-flow kinetics of duplex promoter bending and opening. (A) Stopped-flow kinetic traces of donor fluorescence quenching, acceptor fluorescence increase (FRET signal), and 2-AP fluorescence increase after rapidly mixing 40 nM (final concentration) three-color DNA (A488-NT/2-AP-T-A546) and 100 nM (final concentration) T7 RNAP at 25 °C. The experimental data (rugged curves) fit well to a single-exponential function (smooth curve), as judged from the residuals in panel B. FRET signals of the donor and acceptor were fit simultaneously to a rate constant of 12.9 s^{-1}, while the 2-AP trace was fit separately to a rate constant of 11.3 s^{-1}. (C) T7 RNAP concentration dependence of the observed rate constants of binding (■), bending (▽), and opening (●) of a duplex promoter. DNA bending and opening dependencies were fit to a simple hyperbola with k_{max} values of 190 ± 49 s^{-1} (bending) and 152 ± 17 s^{-1} (opening). All data points were averaged from at least three independent experiments. The binding rate constants were taken from Figure 2B and plotted here for comparison.

measured over a wide T7 RNAP concentration range from 80 to 800 nM (final concentration), and the data are summarized in Figure 4C. The finding that the observed rate constants of DNA bending and opening are indistinguishable over a broad range of T7 RNAP concentrations suggests that the two events occur simultaneously within ~1 ms, the time resolution of the measurement.

In Figure 4C, we compare the observed rate constants of DNA bending and opening at increasing T7 RNAP concentrations with that of DNA binding from the stopped-flow anisotropy measurements. At low concentrations of T7 RNAP, the measured rate constants of the three events coincide. This indicates that at low concentrations of T7 RNAP, the bimolecular association step to form the initial complex limits the entire process of open complex formation. At higher concentrations of T7 RNAP, the bimolecular association step is no longer rate-limiting, whereas the DNA conformational changes become rate-limiting. Therefore, the kinetics of association and DNA conformational changes start to deviate. The observed rate constants of DNA bending and opening steps, unimolecular events, approach at high T7 RNAP concentrations their maximum values. Separate fits of the dependency of the observed rate constants of DNA bending and opening on T7 RNAP concentration to a hyperbolic equation (eq 6) provided a maximal rate constant (k_{max}) of 190 ± 49 s^{-1} for the DNA bending step and a rate constant of 150 ± 17 s^{-1} for the DNA opening step. The latter value is within the range of the DNA opening rate constant previously determined using a 40 bp T7 promoter that spanned residues −21 to +19 (*13*, *14*, *16*).

Stopped-Flow Kinetics of DNA Bending and Opening in the Bubble Promoter. The bubble promoter with contiguous mismatches from position −4 to +2 is a good mimic of the melted DNA in the open complex. Even though the region of residues −4 to +2 of the bubble DNA is premelted, the fluorescence of 2-AP at position −4 in the template increases when the bubble DNA binds to T7 RNAP because the base unstacks upon formation of the binary open complex. Thus, we refer to the event reflected by the 2-AP fluorescence change as DNA opening, bearing in mind that the bubble promoter does not need to be melted in the same way as the duplex promoter. Figure 5A shows typical FRET and 2-AP fluorescence signals when the doubly dye-labeled bubble promoter (40 nM) is rapidly mixed with 200 nM T7 RNAP (both final concentrations). DNA bending as measured by time-dependent FRET changes and opening (or unstacking) as measured by time-dependent 2-AP fluorescence changes follow single-exponential kinetics (Figure 5B) with rate constants of 42 and 40 s^{-1}, respectively. The rate constants of DNA bending and opening are indistinguishable within the time resolution of the method, indicating the simultaneous occurrence of the two events in the six-mismatch bubble promoter as observed with the duplex promoter. The magnitudes of FRET and 2-AP signal changes were larger, however, in the bubble promoter, which is attributed to the complete conversion of the binary complex to the open form. In other words, the final complex of T7 RNAP with the bubble DNA contains only the open complex as the mismatches prevent the reannealing of the bases to form the closed complex.

In contrast to the duplex promoter, the observed rate constants of bending and opening increased linearly instead

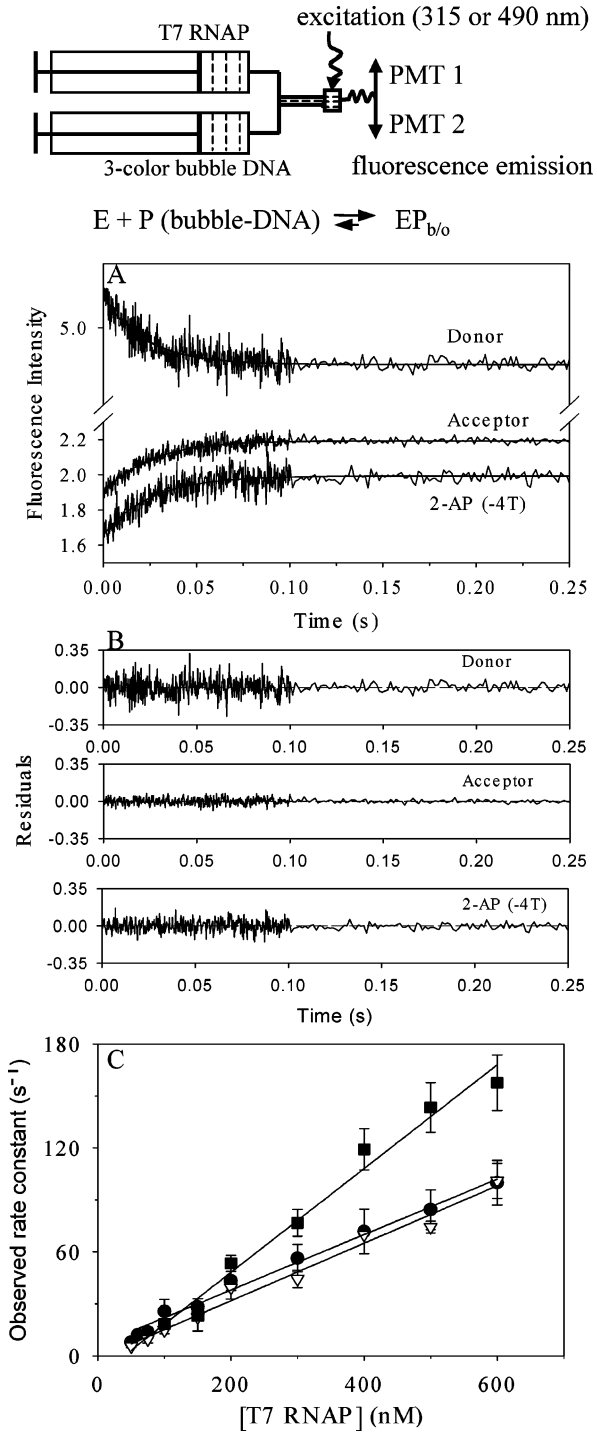

FIGURE 5: Stopped-flow kinetics of bubble promoter bending and opening. (A) Typical traces of stopped-flow FRET and 2-AP fluorescence changes obtained upon mixing 40 nM (final concentration) three-color six-mismatch bubble DNA (A488-mutNT/2-AP-T-A546) with 200 nM (final concentration) T7 RNAP. The donor and acceptor fluorescence changes globally fit to a rate constant of 42 s^{-1}, while the 2-AP fluorescence kinetics fit to a rate constant of 40 s^{-1}. (B) Residual plots show the random distribution of the data around the fitted line throughout the time range, justifying the application of a single-exponential function to fit the data in panel A. (C) Observed rate constants of binding (■), bending (▽), and opening (●) of the bubble DNA increase linearly with an increase in T7 RNAP concentration. The bending and opening dependencies occur with slopes of 165 ± 10 and 167 ± 9 μM^{-1} s^{-1}, respectively. All data were averaged from at least two independent measurements. The binding rate constants were taken from Figure 2D and plotted here for comparison with the bending and opening rate constants.

of hyperbolically as the concentration of T7 RNAP was increased to 600 nM (Figure 5C). The linear dependency indicates that the intrinsic rate constants of DNA bending and opening steps are faster in the bubble promoter than in the duplex promoter. The linear dependency provided second-order rate constants k_{bend} and k_{open} for the bubble promoter represented by the slopes of the linear curves as 165 ± 10 and 167 ± 9 μM^{-1} s^{-1}, respectively. These rate constants are lower than the bimolecular rate constant of bubble DNA binding (299 μM^{-1} s^{-1}), as measured in stopped-flow anisotropy studies. This indicates that open complex formation with the bubble promoter still goes through a multistep kinetic pathway, but with a reduced reverse rate constant and an increased forward rate constant relative to the corresponding values for the duplex promoter. This idea is consistent with the result that the observed bimolecular rate constant of open complex formation increases as the bubble length increases. Thus, k_{open} values are 112 μM^{-1} s^{-1} for the four-mismatched bubble promoter, 167 μM^{-1} s^{-1} for the six-mismatched bubble promoter, 432 μM^{-1} s^{-1} for the eight-mismatched bubble promoter, and 442 μM^{-1} s^{-1} for the partially duplex promoter with a single-stranded template downstream of position −4 (*35*). These results indicate that the stability of the "closed" complex intermediate in this promoter decreases as the bubble length increases. In other words, the energy barrier for T7 RNAP-induced DNA opening must be reduced to a minimum value in the partially duplex promoter and in the eight-mismatched bubble promoter. Therefore, the closed complex is very unstable in the bubble promoters and is rapidly transformed to the open complex, making open complex formation in these premelted promoters essentially a one-step process.

DNA Binding in the Presence of 3′-dGTP. Previously, we made the observation that the initiating nucleotide GTP and its analogue 3′-dGTP drive the open complex formation reaction to completion by stabilizing the open complex by forming a T7 RNAP−promoter−GTP ternary complex (*16*). We observed that the DNA binding rate constant (measured as the 2-AP fluorescence change) increased hyperbolically with an increase in T7 RNAP concentration but was saturated at a much lower value (32 s^{-1}) in the presence of GTP or 3′-dGTP than in the absence of nucleotide (∼180 s^{-1}). Similarly, the observed rate constant of DNA binding *decreased* with an increase in initiating nucleotide concentration. Note that the observed rate constant of DNA binding at saturating T7 RNAP concentrations is the sum of the promoter opening (k_2) and closing (k_{-2}) rate constants (Figure 8). The *decrease* in the observed rate constant as a function of GTP concentration indicated that promoter opening and closing steps are reversible in the duplex promoter, and GTP binding stabilizes the open complex and hence drives the complete conversion of the closed complex to the open complex. Thus, at saturating GTP concentrations, the observed rate constant provides the value of k_2 or the DNA opening rate constant (*37*). In deriving this model, we assumed that GTP binds to only the open complex and does not affect the kinetics of binding of T7 RNAP to the promoter. In this paper, we have developed a stopped-flow fluorescence anisotropy assay for measuring the kinetics of DNA binding, and therefore, we can directly test this assumption. Figure 6 shows the observed DNA binding rate constant (as measured by anisotropy changes) in the presence

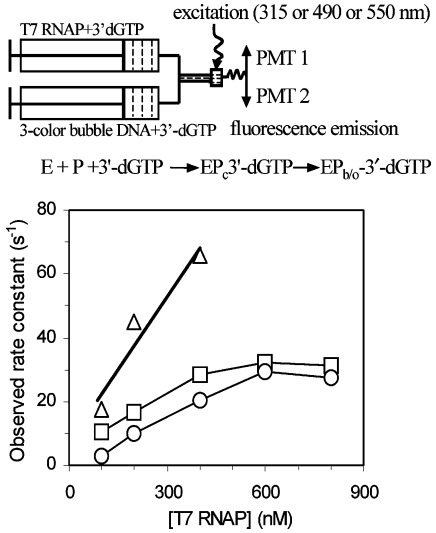

FIGURE 6: Stopped-flow kinetics of duplex promoter binding, bending, and opening in the presence of 3′-dGTP. Single-exponential rate constants of duplex promoter binding (△), bending (○), and opening (□) were obtained from stopped-flow kinetic measurements of A546 anisotropy, FRET, and 2-AP fluorescence signals, respectively. Both DNA and the T7 RNAP solutions contained 0.5 mM 3′-dGTP. A linear fit of the fluorescence anisotropy data yields a k_{on} of 153 μM^{-1} s^{-1}, which is comparable to the on-rate constant of 188 μM^{-1} s^{-1} obtained without 3′-dGTP. The lines connecting the experimental data points of DNA bending and opening rate constants show the nonlinear trend.

of 3′-dGTP as a function of the increasing T7 RNAP concentration. The observed rate constant of anisotropy change increases linearly with an increase in T7 RNAP concentration, and the slope of 154 μM^{-1} s^{-1} in the presence of 3′-dGTP is comparable to the slope of 188 μM^{-1} s^{-1} in the absence of 3′-dGTP. The initiating nucleotide, therefore, does not alter the mechanism of RNAP−DNA association.

To investigate the effect of the initiating nucleotide binding on DNA bending and opening kinetics, stopped-flow FRET and 2-AP fluorescence were measured with the three-color duplex promoter in the presence of 0.5 mM 3′-dGTP. Experiments were conducted at increasing T7 RNAP concentrations in the same manner as in the absence of the nucleotide, and the single-exponential rate constants versus the T7 RNAP concentration are shown in Figure 6. DNA bending and opening kinetics in the presence of 3′-dGTP coincided, and at high T7 RNAP concentrations, the rate constants were saturated at 28 and 32 s^{-1}, respectively. These rate constants are much slower than the rate constants of ~190 s^{-1} observed in the absence of 3′-dGTP. These observations are consistent with previous results that indicated that in the absence of the initiating nucleotides the step of closed to open complex conversion is reversible and the observed rate constant is the sum of the forward and reverse steps (opening and closing, respectively) (*16*). As mentioned above, the observed rate constant is smaller in the presence of 3′-dGTP because of the nearly complete inhibition of the reverse rate constant, k_{-2} (*38*, *39*). The observed rate constant of bending and promoter opening in the presence of 3′-dGTP provided an estimate of the forward rate constant, k_2 (opening), which for simultaneous DNA bending and opening is ~30 s^{-1}. We calculate from the sum of forward and reverse rate constants that reverse rate constant k_{-2} of the closing step is ~149 s^{-1}, in agreement with previously

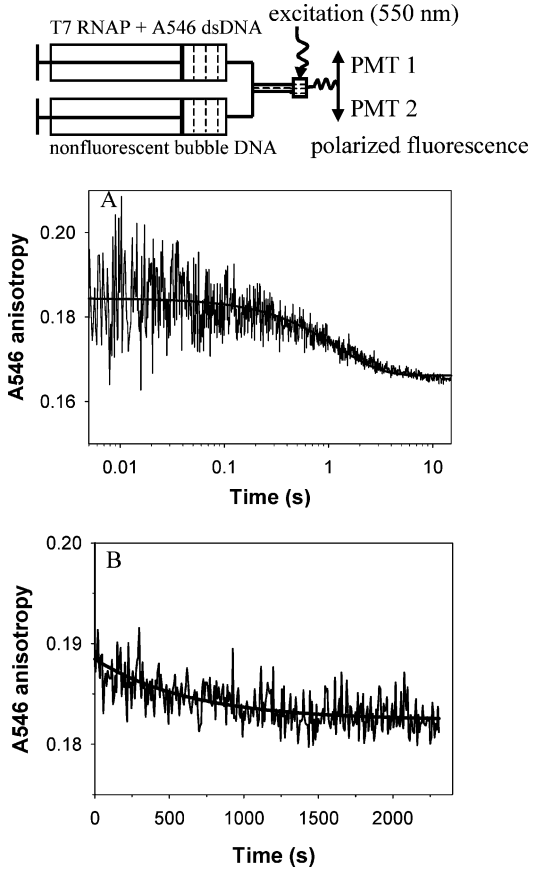

FIGURE 7: Dissociation rate constant of the duplex and six-mismatch promoter as measured by anisotropy changes. (A) A mixture of A546-labeled duplex promoter and T7 RNAP (50 nM) was rapidly mixed with 1 μM unlabeled duplex promoter (both final concentrations). The resulting fluorescence anisotropy decrease (average of 8−10 traces) that was measured through a T-format stopped-flow device fits to the single-exponential function (eq 2) with a rate constant of 0.8 s^{-1}. (B) The DNA-labeled A546 anisotropy was measured after mixing 2 μM (final concentration) unlabeled six-mismatch DNA with a preformed complex of 20 nM A546-labeled bubble DNA and 40 nM T7 RNAP. The slow labeled DNA displacement process was assessed in an L-format steady-state device (PTI QM-3 spectrofluorimeter) with an observation time window of 10 s. The time-dependent fluorescence anisotropy decrease fits to the single-exponential decay equation (eq 2) with a rate constant of 0.09 min^{-1} (solid curve).

determined opening and closing rate constants for the duplex promoter.

Off-Rate of the T7 RNAP−Promoter Complex. The dissociation rate constant (k_{off}) of T7 RNAP from the duplex promoter was determined from the time-dependent decrease in fluorescence anisotropy as the dye-labeled promoter initially bound to T7 RNAP was displaced by unlabeled promoter in a displacement experiment. A preformed complex of A546-labeled duplex promoter and T7 RNAP (50 nM, final concentration) was rapidly mixed with 1 μM unlabeled duplex promoter on the T-format KinTek stopped-flow fluorimeter. Under these experimental conditions, when the labeled duplex promoter dissociates from T7 RNAP, it cannot compete with the excess concentration of unlabeled DNA, and therefore, a decrease in A546 anisotropy is observed as a function of time (Figure 7A). The kinetics of the anisotropy decrease, therefore, provide the dissociation rate constant of the duplex promoter. The time course was fit to a single exponential to obtain a dissociation rate

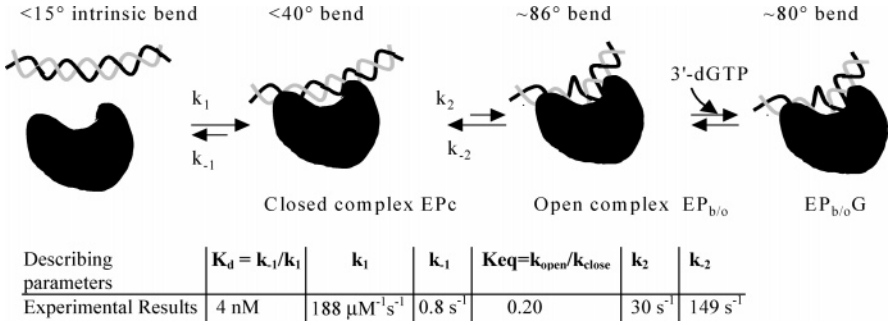

FIGURE 8: Model of promoter DNA binding, bending, and opening during open complex formation. The consensus promoter sequence (P) with a slight intrinsic curvature forms a closed complex (EP_c) upon binding to T7 RNAP. Sharp bending, untwisting, and duplex opening occur around the start site of initiation to form the open complex ($EP_{b/o}$). The open complex is stabilized upon binding of the initiating nucleotides to form the ternary complex ($EP_{b/o}G$). Kinetic parameters obtained from the stopped-flow kinetic studies of fluorescence anisotropy, FRET, and 2-AP fluorescence are shown.

constant of ~0.8 s^{-1}, which is consistent with the off-rate constant recently measured for a 40 bp duplex promoter complex with T7 RNAP using 2-AP fluorescence (*34*). The binding affinity derived from the comparison of k_{off} with k_{on} according to the relationship $K_d = k_{off}/k_{on}$ yields 4.3 nM as the dissociation constant for the T7 RNAP−duplex promoter complex which agrees with the result from equilibrium measurements.

In a similar displacement experiment, the off-rate constant of the bubble DNA from its complex with T7 RNAP was measured on an L-format steady-state spectrofluorimeter. The very slow dissociation allowed us to mix manually an excess of nonfluorescent bubble DNA with a preformed complex of T7 RNAP and the A46-labeled bubble DNA and to measure the fluorescence anisotropy of DNA-labeled A546 in a 10 s time window (Figure 7B). A much smaller off-rate constant ($k_{off} = 0.09$ min^{-1} or 1.5×10^{-3} s^{-1}) for the bubble promoter was derived from fitting the data to a single-exponential decay equation (eq 2). Similarly, slow off-rate constants were measured previously for four- and eight-mismatch bubble promoters (*35*). We concluded that the increased affinity of T7 RNAP for the six-mismatch DNA ($K_d = k_{off}/k_{on} = 5$ pM) is mainly due to the much slower dissociation of the bubble promoter complex with T7 RNAP versus dissociation of the duplex promoter complex with T7 RNAP.

A Refined Model of Open Complex Formation. From the combination of equilibrium and stopped-flow anisotropy, FRET, and 2-AP fluorescence detection of DNA binding, bending, and opening, we propose that the two-step model (Figure 8) is a minimal mechanism that explains the process of promoter opening during transcription initiation by T7 RNAP. The experiments in this paper and the accompanying paper (*48*) provide additional insights into the conformation of the DNA in the closed versus open complex and the temporal coupling of DNA binding, bending, and opening reactions. T7 RNAP binds a consensus promoter sequence at a rapid rate constant of 188 $\mu M^{-1}s^{-1}$ to form a closed complex (EPc) that has a dissociation constant, K_d, of 4 nM. DNA bending in the closed complex is slight, and when the closed complex is converted to the open complex, the DNA is bent more sharply. The DNA bending and opening events occur simultaneously with an apparent rate constant of 179 s^{-1} (an average value obtained from the observed DNA bending and opening rate constants). The observed rate constant is the sum of the forward (k_2) and reverse (k_{-2}) steps. The difference in the free energies of the closed and open complexes (*48*) is small in the absence of initiating nucleotides; hence, the initiation reaction results in an equilibrium mixture of ~20% closed and ~80% open complex. This is also supported by a previously determined value ($k_2/k_{-2} = 0.23$) obtained from the opening and closing rate constants of a 40 bp promoter (*16*) and the 31 bp promoter (*48*). The initiating nucleotides bind to the open complex and without causing any large changes in the DNA conformation drive the open complex reaction to completion.

Coupling of DNA Binding and DNA Conformational Changes in Other Proteins. T7 RNAP represents one of the few examples in which the kinetics of DNA binding and DNA deformation of bending and opening have been extensively characterized. Synchronous DNA binding and bending events have been widely found in several architecture proteins, including the TBP from *Saccharomyces cerevisiae* and humans (*21*, *40*), HMG (*23*), and IHF (*24*). A single concerted event of DNA binding and bending was found also during the recognition of the cognate DNA sequence by EcoRV (*41*). Synchronous DNA binding and base flipping have been observed in methyltransferases such as EcoRI methyltransferase (*27*, *42*), HhaI DNA C5-cytosine methyltransferase (*43*, *44*), and adenine EcoRV methyltransferase (*26*). Only isolated cases in which DNA binding and DNA deformation (such as DNA bending and melting) events are not synchronous have been found; e.g., the binding of T4 DNA polymerase to duplex DNA precedes base unstacking, and this is related to the partitioning of the DNA in the polymerase versus the exonuclease sites for error correction (*45*). The temporal separation between DNA bending and base flipping and the latter event being facilitated by the former one were also proposed for uracil DNA glycosylase recently (*29*). The results with T7 RNAP indicate that the reactions of DNA bending and base pair opening are coupled during open complex formation. Similar observations of increased bending angle and greater opening of the promoter DNA have been made for *Escherichia coli* RNAP·σ^{54} with the *gln*A promoter, where an increase in the extent of DNA bending (from ~49° to ~114°) during the transition from the closed to open complex was observed (*46*), and for the *E. coli* RNAP·σ^{70} holoenzyme with the λP_L promoter (from ~30−70° to ~80−110°) (*47*). Thus, coupling between global deformation of the promoter DNA (bending) and DNA opening may be a general mechanism for prokaryotic RNA polymerases.

REFERENCES

1. McAllister, W. T. (1993) Structure and function of the bacteriophage T7 RNA polymerase (or, the virtues of simplicity), *Cell. Mol. Biol. Res. 39*, 385−391.
2. Sousa, R., and Mukherjee, S. (2003) T7 RNA polymerase, *Prog. Nucleic Acid Res. Mol. Biol. 73*, 1−41.
3. Cheetham, G. M., Jeruzalmi, D., and Steitz, T. A. (1999) Structural basis for initiation of transcription from an RNA polymerase-promoter complex, *Nature 399*, 80−83.
4. Cheetham, G. M., and Steitz, T. A. (1999) Structure of a transcribing T7 RNA polymerase initiation complex, *Science 286*, 2305−2309.
5. Tahirov, T. H., Temiakov, D., Anikin, M., Patlan, V., McAllister, W. T., Vassylyev, D. G., and Yokoyama, S. (2002) Structure of a T7 RNA polymerase elongation complex at 2.9 Å resolution, *Nature 420*, 43−50.
6. Yin, Y. W., and Steitz, T. A. (2002) Structural basis for the transition from initiation to elongation transcription in T7 RNA polymerase, *Science 298*, 1387−1395.
7. Murakami, K. S., Masuda, S., and Darst, S. A. (2002) Structural basis of transcription initiation: RNA polymerase holoenzyme at 4 Å resolution, *Science 296*, 1280−1284.
8. Bushnell, D. A., and Kornberg, R. D. (2003) Complete, 12-subunit RNA polymerase II at 4.1-Å resolution: Implications for the initiation of transcription, *Proc. Natl. Acad. Sci. U.S.A. 100*, 6969−6973.
9. Westover, K. D., Bushnell, D. A., and Kornberg, R. D. (2004) Structural basis of transcription: Separation of RNA from DNA by RNA polymerase II, *Science 303*, 1014−1016.
10. Liu, C., and Martin, C. T. (2001) Fluorescence characterization of the transcription bubble in elongation complexes of T7 RNA polymerase, *J. Mol. Biol. 308*, 465−475.
11. Ujvari, A., and Martin, C. T. (2000) Evidence for DNA bending at the T7 RNA polymerase promoter, *J. Mol. Biol. 295*, 1173−1184.
12. Jia, Y., Kumar, A., and Patel, S. S. (1996) Equilibrium and stopped-flow kinetic studies of interaction between T7 RNA polymerase and its promoters measured by protein and 2-aminopurine fluorescence changes, *J. Biol. Chem. 271*, 30451−30458.
13. Bandwar, R. P., and Patel, S. S. (2001) Peculiar 2-aminopurine fluorescence monitors the dynamics of open complex formation by bacteriophage T7 RNA polymerase, *J. Biol. Chem. 276*, 14075−14082.
14. Bandwar, R. P., Jia, Y., Stano, N. M., and Patel, S. S. (2002) Kinetic and thermodynamic basis of promoter strength: Multiple steps of transcription initiation by T7 RNA polymerase are modulated by the promoter sequence, *Biochemistry 41*, 3586−3595.
15. Ujvari, A., and Martin, C. T. (1996) Thermodynamic and kinetic measurements of promoter binding by T7 RNA polymerase, *Biochemistry 35*, 14574−14582.
16. Stano, N. M., Levin, M. K., and Patel, S. S. (2002) The +2 NTP binding drives open complex formation in T7 RNA polymerase, *J. Biol. Chem. 277*, 37292−37300.
17. Ramstein, J., and Lavery, R. (1988) Energetic coupling between DNA bending and base pair opening, *Proc. Natl. Acad. Sci. U.S.A. 85*, 7231−7235.
18. Travers, A. A. (1990) Why bend DNA? *Cell 60*, 177−180.
19. deHaseth, P. L., and Helmann, J. D. (1995) Open complex formation by *Escherichia coli* RNA polymerase: The mechanism of polymerase-induced strand separation of double helical DNA, *Mol. Microbiol. 16*, 817−824.
20. Perez-Martin, J., Rojo, F., and de Lorenzo, V. (1994) Promoters responsive to DNA bending: A common theme in prokaryotic gene expression, *Microbiol. Rev. 58*, 268−290.
21. Parkhurst, K. M., Brenowitz, M., and Parkhurst, L. J. (1996) Simultaneous binding and bending of promoter DNA by the TATA binding protein: Real time kinetic measurements, *Biochemistry 35*, 7459−7465.
22. Perez-Howard, G. M., Weil, P. A., and Beechem, J. M. (1995) Yeast TATA binding protein interaction with DNA: Fluorescence determination of oligomeric state, equilibrium binding, on-rate, and dissociation kinetics, *Biochemistry 34*, 8005−8017.
23. Jamieson, E. R., Jacobson, M. P., Barnes, C. M., Chow, C. S., and Lippard, S. J. (1999) Structural and kinetic studies of a cisplatin-modified DNA icosamer binding to HMG1 domain B, *J. Biol. Chem. 274*, 12346−12354.
24. Dhavan, G. M., Crothers, D. M., Chance, M. R., and Brenowitz, M. (2002) Concerted binding and bending of DNA by *Escherichia coli* integration host factor, *J. Mol. Biol. 315*, 1027−1037.
25. Allan, B. W., Reich, N. O., and Beechem, J. M. (1999) Measurement of the absolute temporal coupling between DNA binding and base flipping, *Biochemistry 38*, 5308−5314.
26. Gowher, H., and Jeltsch, A. (2000) Molecular enzymology of the EcoRV DNA-(Adenine-N (6))-methyltransferase: Kinetics of DNA binding and bending, kinetic mechanism and linear diffusion of the enzyme on DNA, *J. Mol. Biol. 303*, 93−110.
27. Hopkins, B. B., and Reich, N. O. (2004) Simultaneous DNA binding, bending, and base flipping: Evidence for a novel M.EcoRI methyltransferase-DNA complex, *J. Biol. Chem. 279*, 37049−37060.
28. Su, T. J., Connolly, B. A., Darlington, C., Mallin, R., and Dryden, D. T. (2004) Unusual 2-aminopurine fluorescence from a complex of DNA and the EcoKI methyltransferase, *Nucleic Acids Res. 32*, 2223−2230.
29. Krosky, D. J., Song, F., and Stivers, J. T. (2005) The origins of high-affinity enzyme binding to an extrahelical DNA base, *Biochemistry 44*, 5949−5959.
30. Matlock, D. L., and Heyduk, T. (2000) Sequence determinants for the recognition of the fork junction DNA containing the −10 region of promoter DNA by *E. coli* RNA polymerase, *Biochemistry 39*, 12274−12283.
31. Davanloo, P., Rosenberg, A. H., Dunn, J. J., and Studier, F. W. (1984) Cloning and expression of the gene for bacteriophage T7 RNA polymerase, *Proc. Natl. Acad. Sci. U.S.A. 81*, 2035−2039.
32. King, G. C., Martin, C. T., Pham, T. T., and Coleman, J. E. (1986) Transcription by T7 RNA polymerase is not zinc-dependent and is abolished on amidomethylation of cysteine-347, *Biochemistry 25*, 36−40.
33. Ujvari, A., and Martin, C. T. (1997) Identification of a minimal binding element within the T7 RNA polymerase promoter, *J. Mol. Biol. 273*, 775−781.
34. Tang, G. Q., Bandwar, R. P., and Patel, S. S. (2005) Extended upstream A-T sequence increases T7 promoter strength, *J. Biol. Chem. 280*, 40707−40713.
35. Bandwar, R. P., and Patel, S. S. (2002) The energetics of consensus promoter opening by T7 RNA polymerase, *J. Mol. Biol. 324*, 63−72.
36. Sastry, S. S., and Ross, B. M. (1996) A direct real-time spectroscopic investigation of the mechanism of open complex formation by T7 RNA polymerase, *Biochemistry 35*, 15715−15725.
37. Johnson, K. A. (1992) Transient-State Kinetic Analysis of Enzyme Reaction Pathways, *Enzymes 20*, 1−61.
38. Jia, Y., and Patel, S. S. (1997) Kinetic mechanism of GTP binding and RNA synthesis during transcription initiation by bacteriophage T7 RNA polymerase, *J. Biol. Chem. 272*, 30147−30153.
39. Jia, Y., and Patel, S. S. (1997) Kinetic mechanism of transcription initiation by bacteriophage T7 RNA polymerase, *Biochemistry 36*, 4223−4232.
40. Masters, K. M., Parkhurst, K. M., Daugherty, M. A., and Parkhurst, L. J. (2003) Native human TATA-binding protein simultaneously binds and bends promoter DNA without a slow isomerization step or TFIIB requirement, *J. Biol. Chem. 278*, 31685−31690.
41. Hiller, D. A., Fogg, J. M., Martin, A. M., Beechem, J. M., Reich, N. O., and Perona, J. J. (2003) Simultaneous DNA binding and bending by EcoRV endonuclease observed by real-time fluorescence, *Biochemistry 42*, 14375−14385.
42. Allan, B. W., Garcia, R., Maegley, K., Mort, J., Wong, D., Lindstrom, W., Beechem, J. M., and Reich, N. O. (1999) DNA bending by EcoRI DNA methyltransferase accelerates base flipping but compromises specificity, *J. Biol. Chem. 274*, 19269−19275.
43. Huang, N., Banavali, N. K., and MacKerell, A. D., Jr. (2003) Protein-facilitated base flipping in DNA by cytosine-5-methyltransferase, *Proc. Natl. Acad. Sci. U.S.A. 100*, 68−73.
44. Estabrook, R. A., Lipson, R., Hopkins, B., and Reich, N. (2004) The coupling of tight DNA binding and base flipping: Identification of a conserved structural motif in base flipping enzymes, *J. Biol. Chem. 279*, 31419−31428.
45. Otto, M. R., Bloom, L. B., Goodman, M. F., and Beechem, J. M. (1998) Stopped-flow fluorescence study of precatalytic primer

strand base-unstacking transitions in the exonuclease cleft of bacteriophage T4 DNA polymerase, *Biochemistry 37*, 10156−10163.

46. Rippe, K., Guthold, M., von Hippel, P. H., and Bustamante, C. (1997) Transcriptional activation via DNA-looping: Visualization of intermediates in the activation pathway of *E. coli* RNA polymerase × sigma 54 holoenzyme by scanning force microscopy, *J. Mol. Biol. 270*, 125−138.
47. Rees, W. A., Keller, R. W., Vesenka, J. P., Yang, G., and Bustamante, C. (1993) Evidence of DNA bending in transcription complexes imaged by scanning force microscopy, *Science 260*, 1646−1649.
48. Tang, G.-Q., and Patel, S. S. (2006) *Biochemistry 45*, 4936−4946.

BI052292S